

The Voltage Fed Series Compensation Based ZVZCS Topology and Its Tuning Method for Wireless Electrical Vehicle Battery Charger

Prathyusha Padavala¹, D Dinesh Kumar²

¹PG Scholar, EEE, M.Tech (Electrical Power Systems), Audisankara College of Engineering and Technology, Gudur, India

²Assistant Professor, Department of EEE, Audisankara College of Engineering and Technology, Gudur, India

Abstract: Recently available topologies of high-frequency converter power converter system inductive power transfer (IPT) uses either zero voltage switching (ZVS) or zero-based power converters (ZCS) while keeping the sinusoidal current close to the range limited power transfer. However, achieving ZVS or ZCS for all simultaneous power transfers remains a challenging task for IPT systems. In this article, we developed the zero-voltage zero-current switching (ZVZCS) IPT topology and its proposed switching pattern. ZVS is achieved by enhancing the compensation of the old series and in addition, using an auxiliary network to achieve ZCS. The proposed concept is validated using MATLAB / Simulink-based analogs for battery load resistance.

Keywords: Battery chargers, dc-dc power converters, electric vehicles (EVs), inductive charging, soft switching, wireless power transmission.

1. INTRODUCTION

The increasingly the global economy is facing the destruction of fuel resources and the dangerous disruption of ecosystems. In addition, it has encouraged the emergence of sustainable technologies that lead to new actions for major carbon suppliers, namely, transportation [1], [2]. Therefore, electric vehicles (EVs) were adopted as a solution to reduce the environmental effects caused by carbon-based fuels [2], [3]. In addition, the EVs market opens up new opportunities for people to extend the lifespan of low-cost transportation [1], [3]. In the past, battery technology (BT) and power generation technology were the limits on which to remove EVs from market success. However, BT has emerged with high energy density, low weight, and high efficiency over the past few decades [4]. Additionally, an efficient energy-saving device improves overall performance while in use with a suitable power generation circuit. Dc-dc power configuration with low power loss, durability, reliable power transmission, and additional charging-charge cycles are used by researchers and industry [1] - [4].

Today, efficient, fast chargers are used for short-distance driving with public safety concerns. In the current situation,

inductive power transfer (IPT)-based models are accepted as safe battery charging (BC) solutions during stationary and flexible EV mode. Compensation networks are introduced to prevent impedance of the circuit to improve the overall efficiency of the converter. However, the number of active and passive components of circuits includes configuration difficulties [5]. The right solution also improves driving distance, maintenance cycle, carbon reduction, and end user economy. Therefore, converter selection plays an important role in EV market movement. Therefore, it supports the reduction of environmental problems generated by technology travel issues [6].

Classical series-series capacitor compensation based IPT topology is one of the industry's most widely accepted network systems due to its simple structure and operational stability of various coils [7]. This network produces a low-cost solution but jeopardizes its efficiency, power transmission, high-volume peaks, and controlling different upload accuracy. In [7], a phase control algorithm was introduced to improve efficient bandwidth; however, costs result as a complex control strategy of varying frequency. In [8], the problems generated by the variable frequency are minimized by defining the control boundary at the appropriate frequency range. The control solutions introduced in [7] and [8] only support clam to provide maximum efficiency by maintaining zero power conversion (ZVS) in the IPT system. The development of topological in [9] developed a new coil support network using a central L-C series compensating for both the transmitter and the receiver end. This suspension increases the weight on the side of the car, which is reduced by [10], by placing both coils on the main side. The solution presented in [9] and [10] provides support for magnetic fluctuations in the case of misunderstandings but reduces the aesthetic advantages in calculating and controlling performance. The solution to the problems introduced in [9] and [10] as a remote network to support IPT is addressed [11] by combining the H-bridge high-frequency transformer with the L-C tank network. However, it increases the size, weight, and volume of the entire system while minimizing the maximum value efficiency.

Therefore a solution as the reconstruction of the partial network is introduced [12] - [17] to reduce the problems that have been stripped of the additional sound tank separated by a magnet. In [12] and [13], an equivalent filter network is installed with transformer coils that are freely connected to improve long-term system performance. However, these topologies use magnetically induced inductors, which increase weight, volume, complexity in the tuning process, and reduce efficiency. These issues are resolved in [14] and [15] through unequal compensation using the LCC-C network configuration. Analysis of the claims presented in [12] - [15] is comparatively studied in [16] and [17], and it is found that in the same coil design, the LCC-LCC network is suitable for static IPT and LCC-C I- Powerful IPT. however, it suffers from distortions in the case of car topology and permit variations. Therefore, Zhang et al. [16] and Li et al. [17] direct finding a different solution using the C - C compensation chain. In [18] - [20], a flexible stabilization solution for a wide range of operation, improved efficiency, tightly integrated dc-dc transformer-based converter is introduced. In [21] and [22], an auxiliary network was adopted to improve the performance of sound IPT topology based on [18] - [20]. Consistent losses are increased due to other magnets while stable performance and improved efficiency are achieved. Similarly, a solution for IPT-based IPT series based on C-C was introduced in [23]. At this point of view, IPT with auxiliary cycle can reduce the problems that exist in a network based voltage source inverter (VSI). In this article, the proposed topology uses an old L-C compensation consisting of auxiliary components of small size to make ZVS and current-converted zero (ZCS). The proposed topology provides a constant output voltage even if the input is subject to a wide range of voltages. Current output can be easily controlled from the input side voltage, eliminating the processor requirement for high power control operation, and conversion costs are effectively reduced. The laboratory prototype was designed and tested for battery resistance and full range BC. Figure 1 shows a general overview of the proposed topology in which the two converter phases are controlled using modified pulse width modulation (MPWM) separately. The pulses are produced at 85 kHz to change the frequency in MPWM mode to reach zero-voltage zero-current switching (ZVZCS) to bring power up to 1.1 kW, and performance results are presented. The remaining topic is organized into subsequent sections. The principle of operation of the proposed converter is discussed in Phase II. A circuit design design study is presented in Phase III. Imitation effects are discussed in Section IV. Finally, the conclusion is madeSection V.

2. OPERATING PRINCIPLE OF THE PROPOSED CONVERTER

Active switches S1 - S4 the main side and diodes D5 - D8 on the second side form a bridge H (standard). In addition,

Ca1 and Ca2 act as a potential separator for inputs with Ancillary LA and TA to maintain a slight switching feature in the BC. The primary and secondary side of the circuit are connected by L1 and L2 with C1 and C2, respectively. Conversion performance is controlled using MPWM in [22]. The following considerations are considered in order to understand the operating principle of the proposed converter.

- All active and passive devices include transformer, dc source, switches, diodes, and capacitors suitable for integrating internal switching power and power.
- Resistance to electrical circuit of the inductor and interwinding capacitance of the transformer is ignored.
- The voltage divider capacitors (Ca = Ca1 = Ca2) and CF are large enough to maintain a constant voltage at the input and output terminals of the converter.
- The effects of magnetizing inductance on TA are ignored.

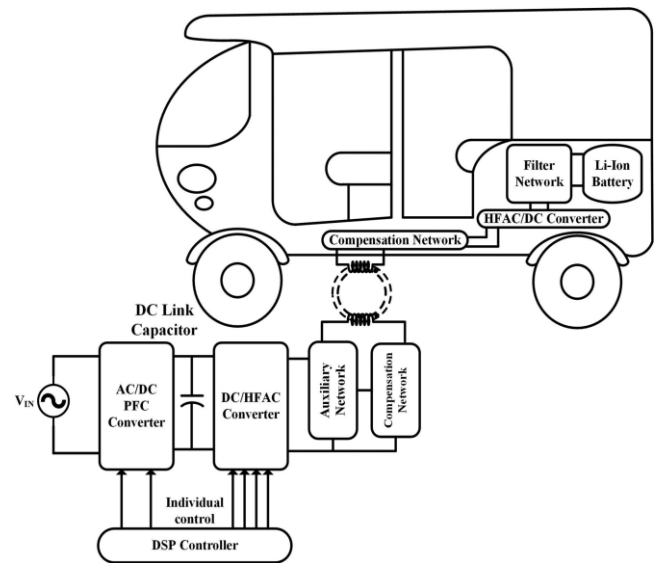


Fig 1 General configuration of wireless battery charger topology

A. Operation of Proposed Converter

The operating principle of the proposed topology in steady state is divided into eight modes (modes I-VIII) as shown in Fig. 2 and the operating waveforms are shown in Fig. 3. 1)

1) *Mode I* ($t_0 \leq t < t_1$), Fig. 2(a): Before the fast t_0 , the lagging current ($I_{L1} + I_{LA}$) flows from D1 and S2, Therefore, with t_0 instantly, switch S1 is turned on with ZVS. In addition, potential differences between AC and CB are created and present I_{LA} start rising from $I_{LA}(t_0)$

$$\left. \begin{aligned} i_{LA} &= \left\{ \begin{aligned} &\text{If } \rightarrow R_{ON(S1-S4)} \neq 0 \\ &\frac{|V_{Ca1} - V_{Ca2}|}{2L_A} T_{ON} - i_{LA}(t_0) \end{aligned} \right. \quad (1) \\ &\left\{ \begin{aligned} &\text{If } \rightarrow R_{ON(S1-S4)} = 0 \\ &|V_{Ca1} - V_{Ca2}| = 0 \parallel i_{LA} = 0 \end{aligned} \right. \end{aligned}$$

2) Mode II ($t1 \leq t < t2$), Fig. 2(b) and (c): Before t_0 , switch S1 is conducting and switch current difference ($i_{S1} - i_{S2}$) is flowing from TA ($ITA1 + ITA2 = ILA$).

Applying KCL at points A and B and using low energy conservation

$$i_{CS1} + i_{CS4} = i_{TA2} + i_{L1} \quad (2)$$

$$2i_{CS1} = i_{L1} + \frac{i_{LA}}{2} \quad (3)$$

At the beginning of this mode, S1 is OFF when S3 is closed, S4 is already OFF, and S2 is still running. The main inductance L1 is now disconnected from the dc power source, and $IL1 + ILA$ starts charging the peracetic capacitor CS1 switch. With faster t_{11} , VCS1 accesses VDC. After t_{11} , IL1 finds its way by forcing a change in ILA. Inductor LA rejects this change and the current start from S2 to S4, which releases CS4. After the CS4 voltage reaches zero, the D4 opens and this free movement leads to a decrease of IS2 to zero or ZCS to the S2 switch.

$$t_{(V_{CS1}=V_{DC})} = \frac{\frac{1}{2}C_{S3}V_{DC} - \left(i_{L1}(t_{1-}) + \frac{i_{LA}(t_{1-})}{2}\right)}{i_{L1}(t) + \frac{i_{LA}(t)}{2}} \quad (4)$$

4) Mode IV ($t3 \leq t < t4$), Fig. 2(f): In this mode of operation, the S4 is turned on by ZVS as D4 is turned on and the voltage across the entire S4 is close to zero. ILA current inductor current grows linearly in a straight line after acquiring its negative peak.

5) Mode V ($t4 \leq t < t5$), Figure 2 (g): In this mode, S3 is unlocked with ZVS. IAB begins to follow the sinusoidal waveform, and the voltage across S3, S4 is zero as its path is completed.

6) Mode VI ($t5 \leq t < t6$), Figure 2 (h) and (i): This mode starts with CLOSING S3, triggering CS3 charging up to VDC in t_{51} . ILA inductor current decreases after receiving its peak and IL1, ILA forces IS4 to lower the ZCS shutdown state.

7) Mode VII ($t6 \leq t < t7$), Figure 2 (j) and (k): In this mode, S4 is OFF in ZCS and VCS4 goes up to VDC in t_{61} . After t_{61} , ILA begins to put the case on the positive side. Diodes D1 and D2

OPEN and the response power to the source.

8) Mode VIII ($t7 \leq t < t8$), Figure 2 (l): During this operation, the S2 switch is ON with ZVS and current shifts from D2 to S2.

B. Operation of the Ancillary Network

The ancillary coil resonant network and transmitter are shown in Fig. 5. The voltage across LA is obtained by using KVL as

$$\begin{aligned} V_{Ca1} &= V_{Ca2} = \frac{V_{DC}}{2} \\ v_{OC} &= v_{LA} = \frac{V_{DC}}{2} - v_{CD} - v_B \\ &= \frac{V_{DC}}{2} - \left(v_A - \frac{V_{DC}}{2}\right) - v_B \\ &= V_{DC} - v_A - v_B \end{aligned}$$

Expression shows the waveform of $v_{OC} = VLA$, which is complimentary of v_{AB} . This shows the current in LA is high for light loading condition and complimentary for heavy loading condition. When the voltage $v_{AB} = VDC$ or $-VDC$ and $v_{Ca1} = v_{Ca2} = \frac{VDC}{2}$ than from expression (9) $VLA = 0$. Therefore, current in inductor LA remains unchanged. The value of i_{LA} is expressed when $v_{Ca1} = v_{Ca2}$ and either S1 -S2 or S3 -S4 in ON state.

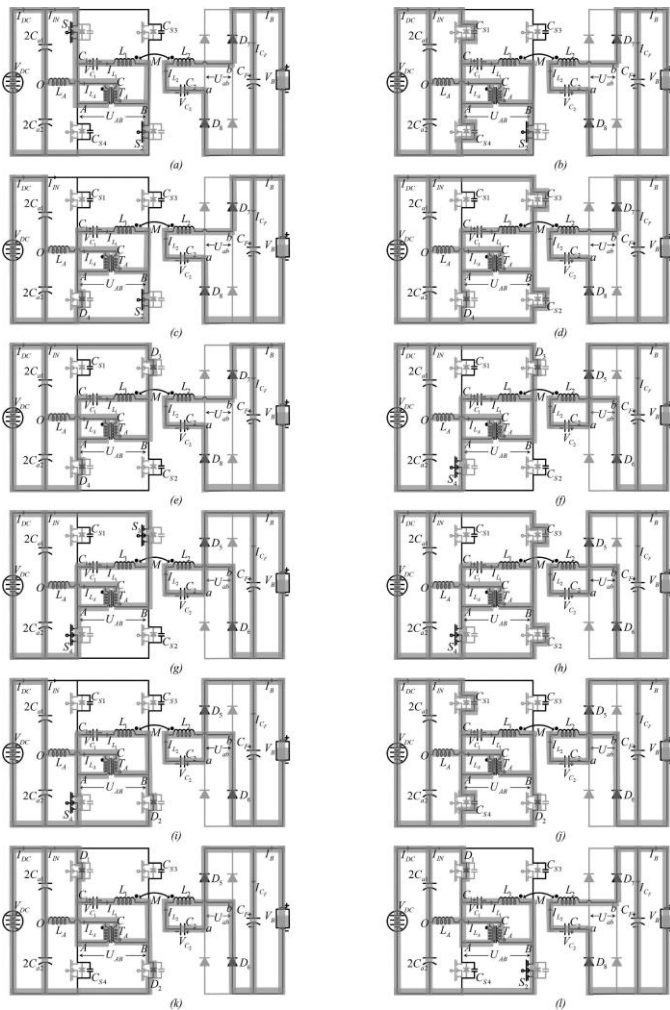


Fig 2 Operating modes of proposed battery charger topology.

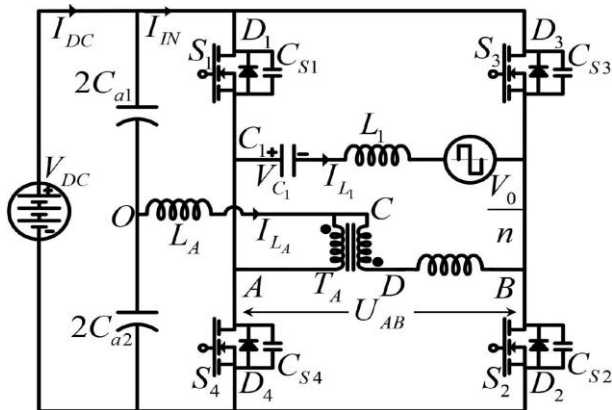


Fig 3 Simplified network with battery load referred at transmitter coil side

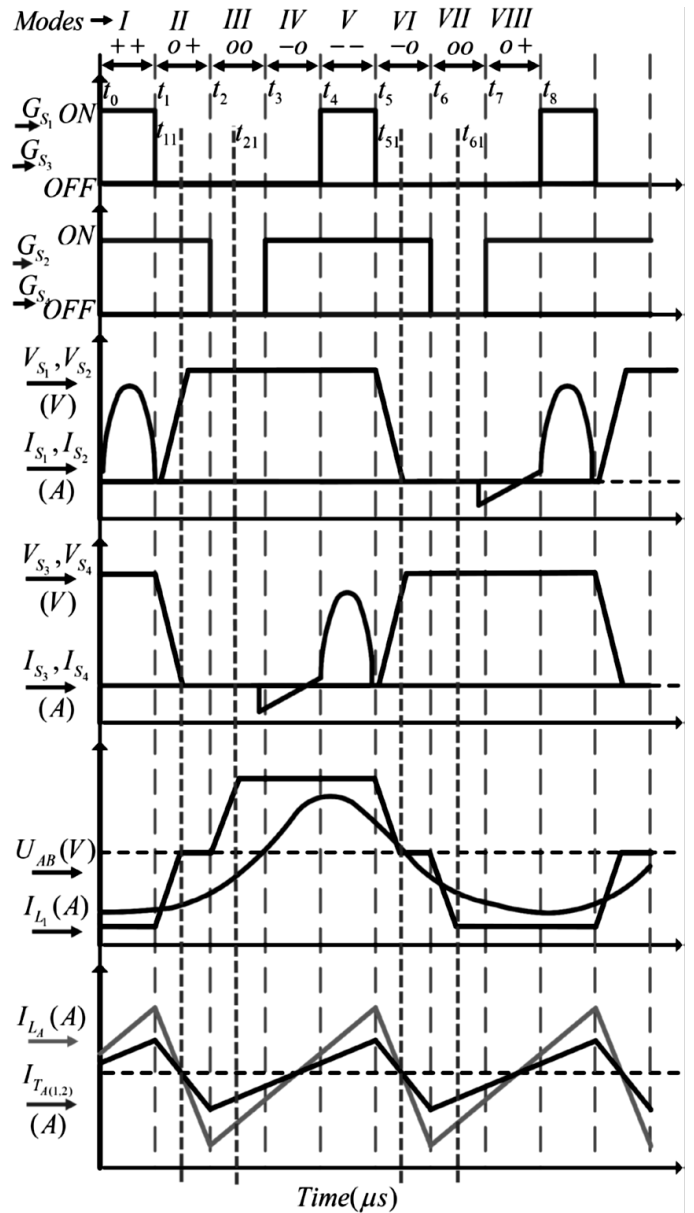


Fig 4 Theoretical operating waveform of proposed wireless converter topology.

3. RESULTS

The operational principle of the topology of the proposed converter is verified by modeling, modeling, and hardware testing. The circuit parameters in the simulation are tuned in the workspace to understand the behavior of the converter.

The simulation of the proposed topology was performed on MATLAB / Simulink using key components, as shown in Figure 10. Unlock ZVS for S1 - S4. in Fig. 4 and Table I. A good source of dc is placed in a series with a resistor (nΩ) and an inductor (nH). MOSFET switches from SimPowerSystem

Library with a power of 0Ω and 870 pF as a snubber used to mimic the H-bridge component of the dc-dc converter. The auxiliary transformer is contracted by a linear transformer and a transmitter, the receiving coils from the mutual inductance. Figure 10 shows the ZVS switch for the ZVS switch S1 to S4, as the voltage across the switch reaches zero, the gate pulse is given to that particular switch to turn it on. In Fig. 11 (a) and (b), ZCS turn-ON switch S2 and S4 are shown. The current from the switch becomes zero before the gate knock is complete. It is therefore said that the proposed wireless converter saves ZCZVS. The maximum voltage of the compensation capacitor is selected by considering the performance of VC1, as shown in Fig. 12. In Figure 13, the input feature of the main network side is shown. These results show the small amount of input dc-link capacitor does not affect the performance of the converter. The function of the BC converter is shown in Fig. 14 (a) - (d). It appears in Fig. 14 (a) and (b) that the interference is minimal, whereas the normal charger interferes with BC voltage and current, which reduces battery life and reduces the efficiency of the charger, while the natural voltage and power supply in Fig. 14 (c) and (d) without the use of a residual circuit. The circuit performance provides 93.5% efficiency with the parameters shown in Table I. The efficiency of the output parameters is controlled by updating the switching frequency and output power is controlled by changing the input voltage..

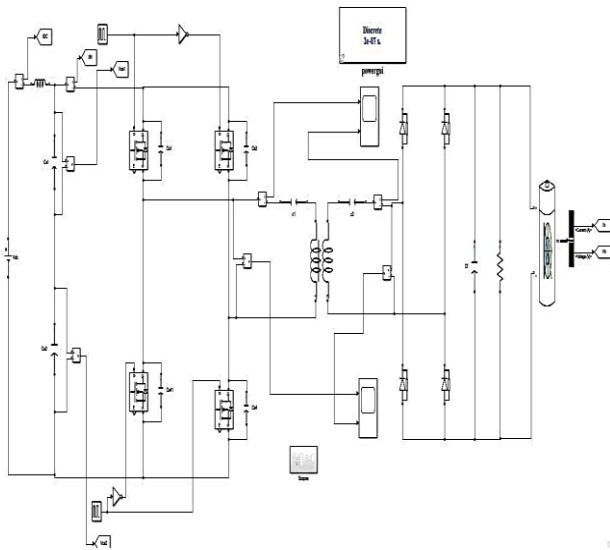


Fig 5 Simulation of Simplified network with battery load refereed at transmitter coil side

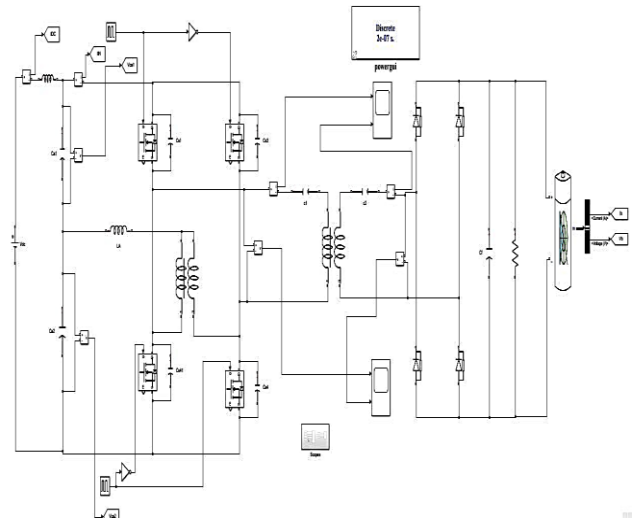


Fig 6 Simulation of Proposed network configuration of EV battery charger

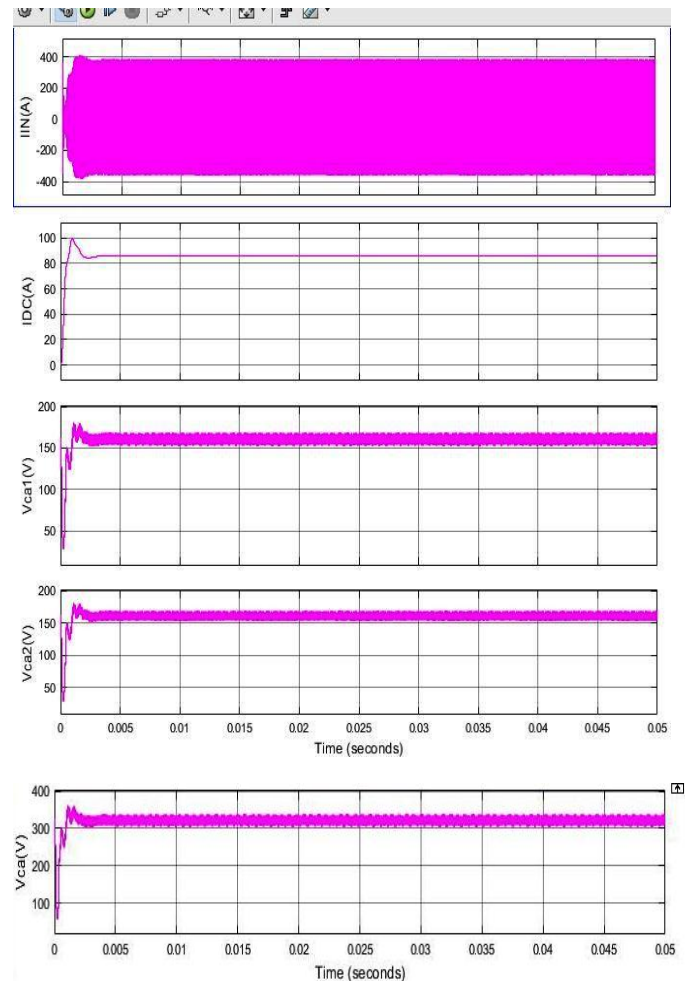


Fig 7 Simulated results of input side characteristic of the primary Network

Table I: Simulation design parameters

Parameters	Symbol	Details
Switching frequency	f	85 kHz
DC link Capacitor	C_{a1}, C_{a2}	47 μF
Auxiliary series inductor	L_A	17.7 μH
Auxiliary transformer ratio	N	1 : 1
Nominal power		550 VA
Nominal voltage		325 V
Nominal leakage inductance		0.4 μH
Magnetizing resistance		20 k Ω
Magnetizing inductance		8 mH
Primary coil inductance	L_1	232 μH
Secondary coil inductance	L_2	232 μH
Coefficient of coupling	k_C	0.16
Mutual inductance	M	37.2 μH
Compensation capacitor primary coil	C_1	15.8 nF
Compensation capacitor secondary coil	C_2	15.6 nF
Electrical series resistance of primary coil and compensation capacitor	R_1	0.2 Ω
Electrical series resistance of secondary coil and compensation capacitor	R_2	0.2 Ω
Switch peracetic capacitance	$C_{S1}, C_{S2}, C_{S3}, C_{S4}$	870 pF
Switch on resistance		270 m Ω
Rectifier diode on state voltage drop		0.45 V
Diode on state resistance		80 m Ω
Filter Capacitance	C_F	47 μF
Battery type		Li-Ion
Battery voltage	V_B	120 V
Load resistance		19 Ω
Switch S_1, S_3 pulse duty cycle		45.5 %
Switch S_2, S_4 pulse duty cycle		48.5 %

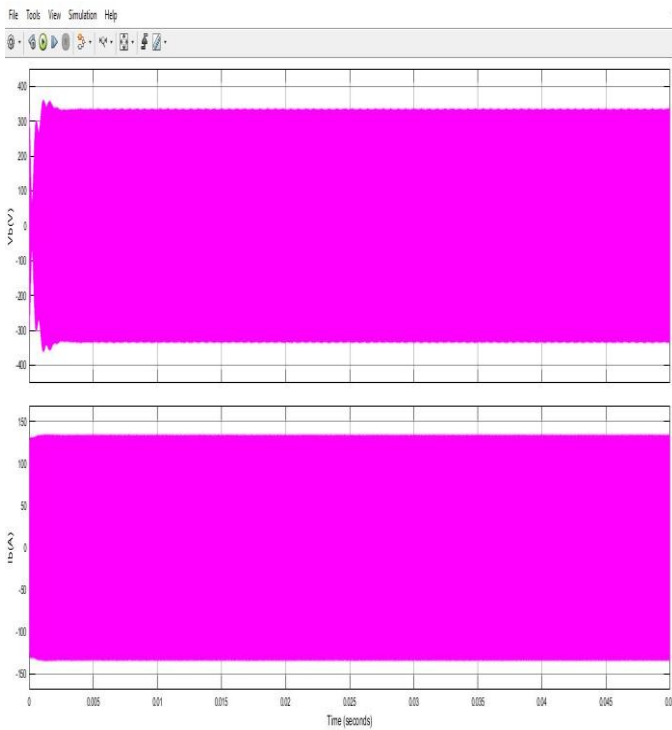


Fig 8 Battery charging voltage and current using the auxiliary circuit

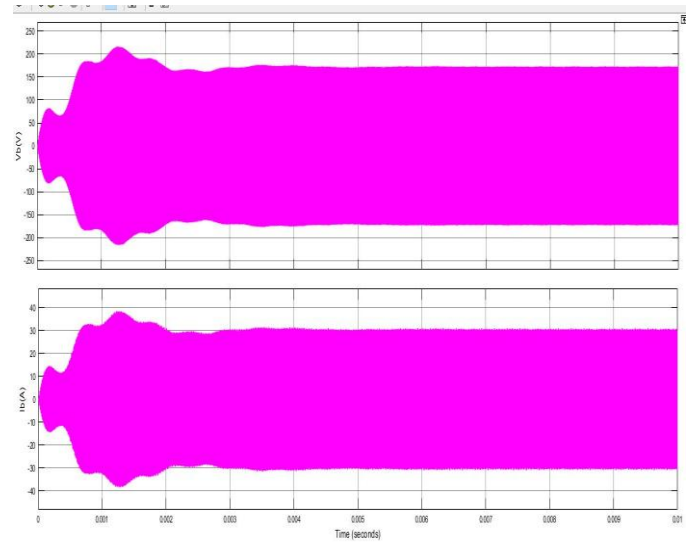


Fig 9 Battery voltage and current without using the auxiliary circuit

4. CONCLUSION

In this article, a series of voltage compensation Fed based on the ZVZCS topology and its method of repairing a battery charger for an electric wireless car is proposed. Appropriate modification is introduced in the full-bridge dc-dc converter, and enhanced functionality with a wide range of input variables is achieved. The need for a high-power processor is eliminated, which further reduces overall costs. Theoretical analysis and modeling were presented to determine ZVZCS with reduced control complexity. The simulation results confirmed the ZVZCS status of the proposed topology for the full width of the load. The solution provided produced a small ripple at the input / output voltage and current while using a low dc connector value, and filter volume values, respectively. An acceptable efficiency of 91.26% is achieved in both battery and resistive loads.

REFERENCES

- [1] M. Granovskii, I. Dincer, and M. A. Rosen, "Economic and environmental comparison of conventional, hybrid, electric and hydrogen fuel cell vehicles," J. Power Sources, vol. 159, no. 2, pp. 1186–1193, 2006.
- [2] S. B. Peterson, J. Whitacre, and J. Apt, "The economics of using plug-in hybrid electric vehicle battery packs for grid storage," J. Power Sources, vol. 195, no. 8, pp. 2377–2384, 2010
- [3] Y. Zhou, M. Wang, H. Hao, L. Johnson, and H. Wang, "Plug-in electric vehicle market penetration and incentives: A

- global review," *Mitigation Adaptation Strategies Global Change*, vol. 20, no. 5, pp. 777–795, 2015.
- [4] B. Nykvist and M. Nilsson, "Rapidly falling costs of battery packs for electric vehicles," *Nature Climate Change*, vol. 5, no. 4, pp. 329–332, 2015.
- [5] W. Zhang and C. C. Mi, "Compensation topologies of high-power wireless power transfer systems," *IEEE Trans. Veh. Technol.*, vol. 65, no. 6, pp. 4768–4778, Jun. 2016.
- [6] K. Mude and K. Aditya, "Comprehensive review and analysis of two-element resonant compensation topologies for wireless inductive power transfer systems," *Chin. J. Elect. Eng.*, vol. 5, no. 2, pp. 14–31, 2019.
- [7] Y. Jiang, L.Wang, Y.Wang, J. Liu, X. Li, and G. Ning, "Analysis, design, and implementation of accurate ZVS angle control for EV battery charging in wireless high-power transfer," *IEEE Trans. Ind. Electron.*, vol. 66, no. 5, pp. 4075–4085, May 2019.
- [8] Y. Jiang, L.Wang, Y.Wang, J. Liu, M.Wu, and G. Ning, "Analysis, design, and implementation of WPT system for EV's battery charging based on optimal operation frequency range," *IEEE Trans. Power Electron.*, vol. 34, no. 7, pp. 6890–6905, Jul. 2019.
- [9] D. H. Tran, V. B. Vu, and W. Choi, "Design of a high-efficiency wireless power transfer system with intermediate coils for the on-board chargers of electric vehicles," *IEEE Trans. Power Electron.*, vol. 33, no. 1, pp. 175–187, Jan. 2018.
- [10] S. Moon and G.-W. Moon, "Wireless power transfer system with an asymmetric four-coil resonator for electric vehicle battery chargers," *IEEE Trans. Power Electron.*, vol. 31, no. 10, pp. 6844–6854, Oct. 2016.
- [11] O. C. Onar, M. Chinthavali, S. L. Campbell, L. E. Seiber, and C. P. White, "Vehicular integration of wireless power transfer systems and hardware interoperability case studies," *IEEE Trans. Ind. Appl.*, vol. 55, no. 5, pp. 5223–5234, Sep./Oct. 2019.
- [12] S. Li, W. Li, J. Deng, T. D. Nguyen, and C. C. Mi, "A double-sided LCC compensation network and its tuning method for wireless power transfer," *IEEE Trans. Veh. Technol.*, vol. 64, no. 6, pp. 2261–2273, Jun. 2015.
- [13] C. Liu, S. Ge, Y. Guo, H. Li, and G. Cai, "Double-LCL resonant compensation network for electric vehicles wireless power transfer: Experimental study and analysis," *IET Power Electron.*, vol. 9, no. 11, pp. 2262–2270, 2016.
- [14] C. Xiao, D. Cheng, and K. Wei, "An LCC-C compensated wireless charging system for implantable cardiac pacemakers: Theory, experiment, and safety evaluation," *IEEE Trans. Power Electron.*, vol. 33, no. 6, pp. 4894–4905, Jun. 2018.
- [15] Y. Chen, H. Zhang, S.-J. Park, and D.-H. Kim, "A switching hybrid LCC-S compensation topology for constant current/voltage EV wireless charging," *IEEE Access*, vol. 7, pp. 133924–133935, 2019.
- [16] Y. Zhang, Z. Yan, T. Kan, Y. Liu, and C. C. Mi, "Modelling and analysis of the distortion of strongly-coupled wireless power transfer systems with SS and LCC-LCC compensations," *IET Power Electron.*, vol. 12, no. 6, pp. 1321–1328, 2019.
- [17] W. Li, H. Zhao, J. Deng, S. Li, and C. C. Mi, "Comparison study on SS and double-sided LCC compensation topologies for EV/PHEV wireless chargers," *IEEE Trans. Veh. Technol.*, vol. 65, no. 6, pp. 4429–4439, Jun. 2016.
- [18] G. N. B. Yadav and N. L. Narasamma, "An active soft switched phase shifted full-bridge dc-dc converter: Analysis, modeling, design, and implementation," *IEEE Trans. Power Electron.*, vol. 29, no. 9, pp. 4538–4550, Sep. 2014.
- [19] M. Pahlevaninezhad, P. Das, J. Drobnik, P. K. Jain, and A. Bakhshai, "A novel ZVZCS full-bridge dc/dc converter used for electric vehicles," *IEEE Trans. Power Electron.*, vol. 27, no. 6, pp. 2752–2769, Jun. 2012.
- [20] V. R. K. Kanamarlapudi, B. Wang, P. L. So, and Z. Wang, "Analysis, design, and implementation of an APWM ZVZCS full-bridge dc-dc converter for battery charging in electric vehicles," *IEEE Trans. Power Electron.*, vol. 32, no. 8, pp. 6145–6160, Aug. 2017.
- [21] J. K. Nama, M. Srivastava, and A. K. Verma, "Modified inductive power transfer topology for electrical vehicle battery charging using auxiliary network to achieve zero-voltage switching for full load variations," *IET Power Electron.*, vol. 12, no. 10, pp. 2513–2522, 2019.
- [22] M. Srivastava, P. S. Tomar, and A. K. Verma, "A modified duty cycle frequency control soft switching of full bridge dc-dc converter for electric vehicle battery charging,"
- [23] J. K. Nama, P. S. Tomar, M. Srivastava, and A. K. Verma, "An efficient wireless topology for electric vehicle battery charging," in *Proc. 8th IEEE India Int. Conf. Power Electron.*, 2018, pp. 1–6.

- [24] Parashar Vidyut Udyog, Litz Wire—pdf catalogue, 2020. [Online]. Available: <https://pdf.indiamart.com/impdf/9435952930/MY-10389389/litz-wire.pdf>
- [25] Magnetics International, Kool M μ Hf Powder Cores, 2020. [Online]. Available: <https://www.mag-inc.com/Media/Magnetics/File-Library/Product%20Literature/Powder%20Core%20Literature/Magnetics-Kool-M%20b5-H%2092-Bulletin.pdf>
- [26] Magnetics International, Ferrite Cores—Toroids | Shapes | Pot Cores, 2020. [Online]. Available: <https://www.mag-inc.com/getattachment/Products/Ferrite-Cores/Learn>